Notes on Numerical Fluid Mechanics and Multidisciplinary Design 150

Geert Degrande · Geert Lombaert · David Anderson · Paul de Vos · Pierre-Etienne Gautier · Masanobu Iida · James Tuman Nelson · Jens C. O. Nielsen · David J. Thompson · Thorsten Tielkes · David A. Towers *Editors*

Noise and Vibration Mitigation for Rail Transportation Systems

Proceedings of the 13th International Workshop on Railway Noise, 16–20 September 2019, Ghent, Belgium

Springer

Notes on Numerical Fluid Mechanics and Multidisciplinary Design

Volume 150

Founding Editor

Ernst Heinrich Hirschel, Zorneding, Germany

Series Editor

Wolfgang Schröder, Aerodynamisches Institut, RWTH Aachen, Aachen, Germany

Editorial Board

Bendiks Jan Boersma, Delft University of Technology, Delft, The Netherlands

Kozo Fujii, Institute of Space & Astronautical Science (ISAS), Sagamihara, Kanagawa, Japan

Werner Haase, Hohenbrunn, Germany

Michael A. Leschziner, Department of Aeronautics, Imperial College, London, UK

Jacques Periaux, Paris, France

Sergio Pirozzoli, Department of Mechanical and Aerospace Engineering, University of Rome 'La Sapienza', Roma, Italy

Arthur Rizzi, Department of Aeronautics, KTH Royal Institute of Technology, Stockholm, Sweden

Bernard Roux, Ecole Supérieure d'Ingénieurs de Marseille, Marseille CX 20, France

Yurii I. Shokin, Siberian Branch of the Russian Academy of Sciences, Novosibirsk, Russia

Managing Editor

Esther Mäteling, RWTH Aachen University, Aachen, Germany

Notes on Numerical Fluid Mechanics and Multidisciplinary Design publishes state-of-art methods (including high performance methods) for numerical fluid mechanics, numerical simulation and multidisciplinary design optimization. The series includes proceedings of specialized conferences and workshops, as well as relevant project reports and monographs.

More information about this series at http://www.springer.com/series/4629

Geert Degrande · Geert Lombaert ·
David Anderson · Paul de Vos ·
Pierre-Etienne Gautier · Masanobu Iida ·
James Tuman Nelson · Jens C. O. Nielsen ·
David J. Thompson · Thorsten Tielkes ·
David A. Towers
Editors

Noise and Vibration Mitigation for Rail Transportation Systems

Proceedings of the 13th International Workshop on Railway Noise, 16–20 September 2019, Ghent, Belgium

Springer

Editors
Geert Degrande
Department of Civil Engineering
KU Leuven
Leuven, Belgium

David Anderson
Acoustic Studio
Stanmore, NSW, Australia

Pierre-Etienne Gautier
SNCF Réseau
La Plaine Saint Denis, France

James Tuman Nelson
Wilson, Ihrig & Associates
Emeryville, CA, USA

David J. Thompson
Institute of Sound and Vibration Research
University of Southampton
Southampton, UK

David A. Towers
Cross-Spectrum Acoustics Inc
Burlington, MA, USA

Geert Lombaert
Department of Civil Engineering
KU Leuven
Leuven, Belgium

Paul de Vos
SATIS
Weesp, The Netherlands

Masanobu Iida
Research & Development Promotion Division
Railway Technical Research Institute
Tokyo, Japan

Jens C. O. Nielsen
Department of Mechanics and Maritime Sciences
Chalmers University of Technology
Gothenburg, Sweden

Thorsten Tielkes
DB Systemtechnik GmbH
München, Germany

ISSN 1612-2909 ISSN 1860-0824 (electronic)
Notes on Numerical Fluid Mechanics and Multidisciplinary Design
ISBN 978-3-030-70288-5 ISBN 978-3-030-70289-2 (eBook)
https://doi.org/10.1007/978-3-030-70289-2

© Springer Nature Switzerland AG 2021
This work is subject to copyright. All rights are reserved by the Publisher, whether the whole or part of the material is concerned, specifically the rights of translation, reprinting, reuse of illustrations, recitation, broadcasting, reproduction on microfilms or in any other physical way, and transmission or information storage and retrieval, electronic adaptation, computer software, or by similar or dissimilar methodology now known or hereafter developed.
The use of general descriptive names, registered names, trademarks, service marks, etc. in this publication does not imply, even in the absence of a specific statement, that such names are exempt from the relevant protective laws and regulations and therefore free for general use.
The publisher, the authors and the editors are safe to assume that the advice and information in this book are believed to be true and accurate at the date of publication. Neither the publisher nor the authors or the editors give a warranty, expressed or implied, with respect to the material contained herein or for any errors or omissions that may have been made. The publisher remains neutral with regard to jurisdictional claims in published maps and institutional affiliations.

This Springer imprint is published by the registered company Springer Nature Switzerland AG
The registered company address is: Gewerbestrasse 11, 6330 Cham, Switzerland

Preface

This volume contains the peer-reviewed contributions to the 13th International Workshop on Railway Noise (IWRN13), which took place in Ghent, Belgium, during 16–20 September 2019. The workshop was hosted by the Structural Mechanics Section of the Department of Civil Engineering of KU Leuven in collaboration with the Conference and Events Office of KU Leuven.

IWRN13 was also made possible by the support of Pandrol (Gold sponsor), Infrabel and Strukton Rail (Silver sponsors) and D2S International, GeoSIG and TUC Rail (Bronze sponsors).

The workshop was attended by 159 delegates and eight accompanying persons from 23 countries on four continents: Germany (20), Belgium (19), France (19), UK (17), China (16), The Netherlands (10), Sweden (8), Australia (6), Spain (6), Austria (5), Japan (5), Switzerland (5), USA (5), Czech Republic (3), Singapore (3), Denmark (2), Hong Kong (2), Italy (2), Norway (2), Canada (1), Hungary (1), South Korea (1) and Romania (1).

In comparison with other modes of transportation, rail transport is safe and environmentally friendly and is generally described as the most sustainable mode for regional and international transport. However, it is also recognised that the environmental impact of railway noise and vibration needs to be further reduced.

Since the first IWRN in 1976, held in Derby (United Kingdom) with 35 delegates, the workshop series has been established as a regular event (held every three years) that brings together the leading researchers and engineers in all fields related to railway noise and vibration. The IWRN workshops have contributed significantly to the understanding and solution of many problems in railway noise and vibration, building a scientific foundation for reducing environmental impact by air-borne, ground-borne and structure-borne noise and vibration.

Following the tradition from previous workshops, the scientific programme of IWRN13 was held as a single session event over three and a half days. The programme contained two keynote lectures, 55 oral presentations and 37 poster presentations. The poster sessions commenced with three-minute rapid-fire oral presentations to introduce each poster, and these sessions were very well attended.

This volume contains the peer-reviewed papers from 78 of these presentations, including two keynote papers on wheel-rail impact loads, noise and vibration and on interior noise in railway vehicles. IWRN13 covered nine different themes: high-speed rail and aerodynamic noise; interior noise; policy, regulation and perception; predictions, measurements and modelling; rail roughness, corrugation and grinding; squeal noise; structure-borne noise and ground-borne vibration; wheel and rail noise and bridge noise and vibration.

In parallel with the scientific programme, eight companies gathered at IWRN13 to display their technology and services in the area of railway noise and vibration: Pandrol, GeoSIG, Enmo, Gerb, Sekisui, Sigicom, 4Silence and ACSOFT.

There is no formal organisation behind the IWRN but rather an informal, committed international committee. It supports the chairman during the preparation process with the experience and expertise of its members. Assistance is given to formulate the scientific programme by reviewing the submitted abstracts, to act as session chairmen and to act as peer reviewers and editors of the IWRN proceedings published in this volume.

The international committee is grateful to Kristien Van Crombrugge, Ann Zwarts, Kurt Scherpereel, Cédric Van hoorickx and Pieter Reumers of the local committee for their great commitment and care in organising the workshop.

The editors of this volume are grateful to Professor Wolfgang Schröder as the general editor of the "Notes on Numerical Fluid Mechanics and Multidisciplinary Design" and also to the staff of the Springer Verlag (in particular, Dr. Leontina Di Cecco) for the opportunity to publish the proceedings of the IWRN13 workshop in this series. Note that previous workshop proceedings has also been published in this series (IWRN9 in volume 99, IWRN10 in volume 118, IWRN11 in volume 126 and IWRN12 in volume 139).

We hope that this volume will be used as a "state-of-the-art" reference by scientists and engineers involved in solving noise and vibration problems related to railway traffic.

August 2020

Geert Degrande
Geert Lombaert
David Anderson
Paul de Vos
Pierre-Etienne Gautier
Masanobu Iida
James Tuman Nelson
Jens C. O. Nielsen
David J. Thompson
Thorsten Tielkes
David A. Towers

Contents

Keynote Lectures

Wheel–Rail Impact Loads, Noise and Vibration: A Review of Excitation Mechanisms, Prediction Methods and Mitigation Measures

Jens C. O. Nielsen[1(✉)], Astrid Pieringer[2], David J. Thompson[3], and Peter T. Torstensson[4]

[1] Department of Mechanics and Maritime Sciences, Division of Dynamics/CHARMEC, Chalmers University of Technology, 412 96 Gothenburg, Sweden
jens.nielsen@chalmers.se
[2] Department of Architecture and Civil Engineering, Division of Applied Acoustics/CHARMEC, Chalmers University of Technology, 412 96 Gothenburg, Sweden
[3] Institute of Sound and Vibration Research, University of Southampton, Southampton SO17 1BJ, UK
[4] Swedish National Road and Transport Research Institute, Regnbågsgatan 1, 417 55 Gothenburg, Sweden

Abstract. Railway noise and ground-borne vibration induced by wheel–rail impact loads are generated by discrete wheel/rail surface irregularities or local deviations in the nominal wheel–rail contact geometry. On the running surface of a rail, a discrete irregularity can be inherent to the railway design, for example at crossings or insulated joints. On the wheel or rail, the irregularity could also be the result of surface damage due to rolling contact fatigue cracking or a consequence of wheel sliding without rolling. This review describes the mechanisms of wheel–rail impact generated by wheel flats, rail joints and crossings. These can be a source of locally increased noise and vibration levels and increased annoyance, as well as of damage to vehicle and track components. The wheel–rail excitation at such irregularities, as indicated by the vertical wheel centre trajectory, leads to an abrupt change of momentum, potentially causing a momentary loss of wheel–rail contact followed by an impact on the rail. The resulting loading is a transient and often periodically repeated event exciting vibration in a wide frequency range with most of the energy concentrated below about 1 kHz. For the numerical prediction of high-magnitude transient loading and situations potentially leading to loss of contact, a non-linear wheel–rail contact model is required, implying that the simulation of contact force is carried out in the time domain. To avoid the need for large, computationally expensive models, a hybrid approach has been developed in which the time history of the contact force is transformed into an equivalent roughness spectrum; this is used as input to frequency-domain models for the prediction of noise and vibration. Since the excitation mechanism is similar to that for rolling noise, the same types of measures to mitigate wheel and track vibration can be applied. However, the main priority should be to control the irregularity by design and regular maintenance.

© Springer Nature Switzerland AG 2021
G. Degrande et al. (Eds.): *Noise and Vibration Mitigation for Rail Transportation Systems*, NNFM 150, pp. 3–40, 2021.
https://doi.org/10.1007/978-3-030-70289-2_1

Keywords: Wheel–rail impact noise and vibration · Excitation mechanisms · Mitigation

1 Introduction

In comparison with most other modes of transportation, railway traffic is safer and more environmentally friendly, and is generally described as the most sustainable mode for regional and international transport. However, with higher train speeds and axle loads, increased traffic density and sometimes a growing maintenance debt due to increasing rates of wheel and rail profile degradation, the issues of railway noise and vibration are becoming increasingly important. This results in a growing number of complaints from residents near existing lines as well as resistance to the building of new railways.

The many different forms of railway noise include rolling noise induced by the acoustic roughness (unevenness) on the rolling surface of wheels and rails, aerodynamic noise generated by air flow and turbulence around the train at high speeds, squeal noise due to frictional instability in the tangential wheel–rail contact in sharp radius curves, impact noise at discrete wheel/rail surface irregularities, brake noise, engine noise, etc. [1]. The understanding and modelling of the mechanisms of these noise sources have improved significantly over recent decades and solutions for mitigation are available and widespread. The state-of-the-art on rolling noise has been presented for example in refs. [2, 3], on aerodynamic noise in refs. [4, 5], and on squeal noise in refs. [6, 7]. An early contribution to the prediction of wheel–rail impact noise was presented by Vér et al. [8] and later extended by Remington [6]. Ground-borne vibration generated by railway traffic was surveyed in refs. [9, 10]. Several of these reviews were initiated and first presented within the International Workshop on Railway Noise (IWRN) community. Following this tradition, this paper is a review on noise and vibration generated by wheel–rail impact.

In this review paper, the term *impact* refers to a situation with a transient vertical wheel–rail contact loading resulting in a maximum of the contact force that is high relative to the static wheel load but not necessarily leading to a momentary loss of contact.

The impact between wheel and rail is generated due to a severe wheel/rail surface irregularity or a local deviation in the nominal wheel–rail contact geometry. In extreme cases this can also lead to a momentary loss of wheel–rail contact. A discrete irregularity on the running surface of a rail can be inherent to the railway design. This is the case for crossings, required to allow for intersecting tracks, and for insulated rail joints used to divide the track electrically for train detection as part of the signalling system. Discrete irregularities can also be the result of surface damage due to rolling contact fatigue of wheel and rail leading to crack propagation and subsequent breaking out of pieces of wheel/rail material (shelling, squats, etc.), or a consequence of wheel sliding without rolling (wheel flats).

Wheel–rail impact loads due to discrete surface irregularities lead to the generation of noise and ground-borne vibration. Furthermore, if the wheels and rails are not maintained on time, these irregularities may lead to damage to the track or vehicle due

to repeated impact loading and plastic deformation, leading to a further growth of the irregularities. In this paper, wheel flats, rail joints and crossings will be used as three examples of irregularities generating wheel–rail impact loads, noise and vibration. The characteristics of each of these irregularities are briefly described in Sect. 2. Examples of field measurements quantifying the consequences of wheel–rail impact are presented in Sect. 3. Impact noise can be considered as an extreme form of rolling noise, in which the prescribed relative wheel–rail vertical displacement excitation is generated by a discrete irregularity. On this note, prescribed wheel trajectories based on simple formulae and used as input to models of dynamic wheel–rail interaction are surveyed in Sect. 4. Models of wheel–rail contact and dynamic wheel–rail interaction are treated in Sects. 5 and 6. Impact loads, noise and vibration are discussed in Sects. 7 and 8, while mitigation measures are summarised in Sect. 9.

2 Discrete Wheel/Rail Surface Irregularities

2.1 Wheel Flats

A discrete wheel tread defect is a local deviation from the nominal wheel radius along a short section of the wheel circumference. This deviation introduces a radial irregularity that, for each wheel revolution, may generate an impact load in the wheel–rail contact. One common discrete tread defect, the wheel flat, is developed due to sliding (without rolling) of the wheel along the rail, see Fig. 1(a). The reason for the sliding may be that the brakes are poorly adjusted, frozen or defective, or that the braking force is too high in relation to the available wheel/rail friction [11]. Contaminations on the rail surface, such as leaves, grease, frost and snow will reduce the friction coefficient and may aggravate the problem. As a consequence of the sliding, part of the wheel tread is worn off and locally the wheel temperature is raised significantly due to the dissipated friction energy. When the wheel starts rolling again, this is followed by a rapid cooling due to conduction into the large steel volume surrounding the flat. This may lead to the formation of martensite and residual stresses [11–13].

The initial flat with sharp edges will soon be transformed into a longer flat with rounded edges because of wear and plastic deformation of the wheel material at subsequent impacts with the rail, whereas the depth at the centre of the flat can be unchanged [14]. However, if martensite is formed, cracks may initiate and propagate in the brittle material due to the rolling contact loading and the repeated impacts. Due to the tensile residual stresses in the surrounding material, cracks may grow to considerable depths and pieces of the wheel tread may detach aggravating the irregularity.

Surface or subsurface initiated rolling contact fatigue resulting in cracking and the breaking out of clusters of pieces of tread material is another type of discrete wheel tread defect that may result in higher impact loads than generated by a wheel flat [15].

2.2 Rail Joints

Rail joints are used to allow for the expansion of rails in hot weather conditions (expansion joints) or for signalling purposes in continuously welded track (insulated joints).

One example of an insulated rail joint is shown in Fig. 1(b). To ensure the insulation, a nylon material is used in the gap between the two rails. In this example, the joint has been assembled using two 0.9 m long fish-plates (joint bars), one on each side of the rail, also separate from the rail by nylon insulators. The mass of the two fish-plates with six bolts is about 50 kg [16].

To allow for variations in temperature, the gap width between two rails in a modern track is 0–20 mm. Besides a small vertical misalignment between the two rails, there may be a vertical dip in the rail generating a dip angle at the joint. Welding of rails in the field may result in a similar cusp-like discontinuity [17]. It has been suggested that the dip can be approximated by a symmetric quadratic function on each side of the joint, see Sect. 4.2. Severe deformation of the two rail ends due to repeated impact loading and/or detached material is a safety issue as the insulating function may be lost.

In addition to the geometric irregularity, the joint leads to a local variation in dynamic track stiffness due to the two free rail ends and the weight and stiffness added by the fish-plate assembly. An example of a model for simulation of dynamic interaction between a vehicle and a track with a joint is shown in Fig. 2. The variation in beam properties $p(x)$ of the coupled rail/fish-plate structure is schematically sketched in the figure, where for example the rail bending stiffness changes from its nominal value to a higher value due to the coupling with the fish-plates. Over the gap, the rail bending stiffness, then only supplied by the fish-plates, drops to a lower value.

Examples of measured and calculated track receptances are presented in ref. [16]. For frequencies above around 300 Hz, the fish-plate assembly leads to an increased dynamic stiffness (lower receptance) compared to nominal track. The track resonance at around 250 Hz, where there is a relative motion of the rail and sleepers, is shifted to a lower frequency because of the mass of the assembly. Also, the receptance at the pinned-pinned resonance at around 1000 Hz is influenced by the joint.

2.3 Crossings

A fixed crossing, see Fig. 1(c), allows for trains to pass over two intersecting tracks. Since two different wheel paths intersect at one point, there is a flangeway on either side of the crossing nose to allow the wheel flanges to pass through the crossing in either the through route or the diverging route. The rails are therefore split into a crossing nose and two wing rails, see also Fig. 3. In the facing move (travelling direction from switch to crossing), the wheels roll on the closure rails towards the crossing. In the trailing move the traffic travels in the opposite direction.

For nominal wheel and rail profiles, according to design, the transfer of a wheel from the wing rail to the crossing nose (or vice versa) in the crossing panel should be relatively smooth. However, wheel profiles with different stages of profile wear will make the transition between wing rail and crossing nose at different positions along the crossing [18]. Wheels should not make contact near the tip of the crossing nose where it is too thin to carry the wheel load, see Fig. 1(c). For the same reason, situations where the field side of the wheel tread is making contact with the gauge corner of the wing rail should be avoided. These two constraints determine the length of the transition zone.

The conicity of the wheel in combination with the variation in rail geometry along the crossing panel, where the stock rail is curved laterally into the wing rail and the crossing

(a)

(b)

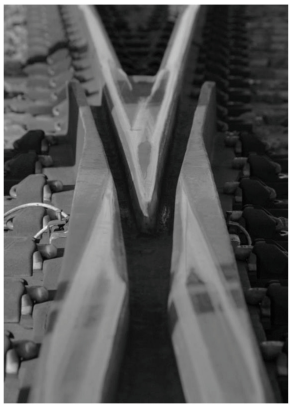

(c)

Fig. 1. (a) Wheel flat. Photo by Robert Fröhling, Transnet, South Africa. (b) Insulated rail joint with fish-plate assembly, from [16]. (c) Fixed crossing with crossing nose and two wing rails. Photo by Björn Pålsson, Chalmers University of Technology, Sweden.

nose has a vertical inclination, results in a wheel–rail excitation that is characterised by a dip angle in the vertical wheel centre trajectory, see Sect. 4.3. Wheels with different stages of profile wear result in different trajectories with different dip angles in the

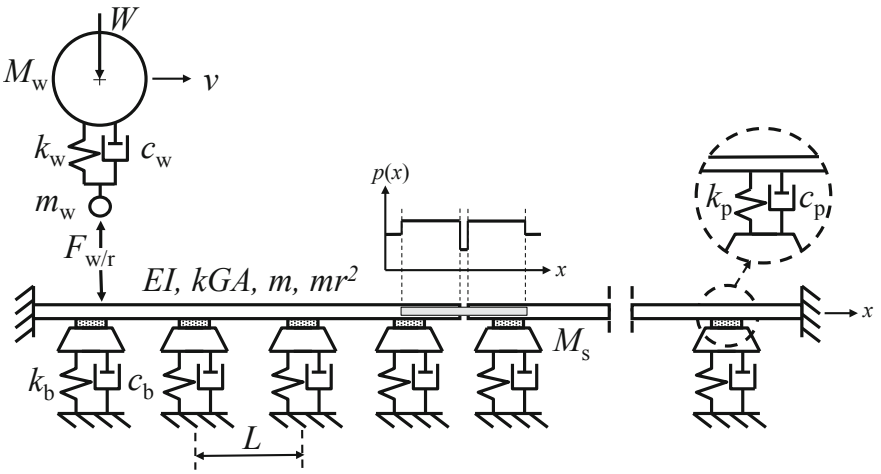

Fig. 2. Sketch of model for simulation of vertical dynamic interaction between a wheelset and a track with a fish-plated joint.

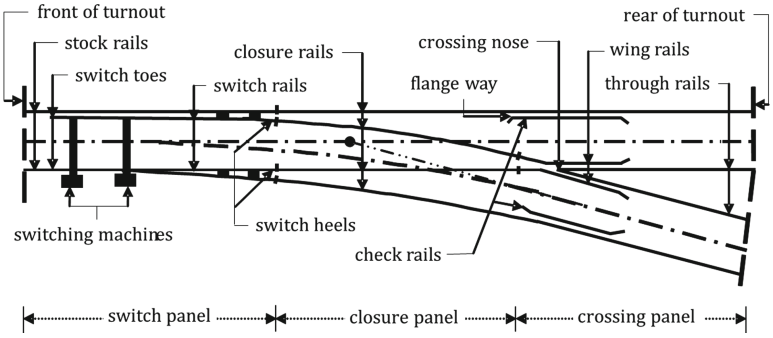

Fig. 3. Sketch of a switch & crossing (S&C) with notations. From [20].

same crossing. Wheel profiles deviating from the design conditions will generate severe impact loads. In particular, this is the case for hollow worn wheel profiles [19, 20].

In crossings, the variation in length of sleepers and the complex arrangement with a combination of several rails lead to a variation in track stiffness and mass [21]. Moreover, the symmetry of plain line track is lost leading to a significant variation and difference in track vertical stiffness at the inner and outer rails, see Fig. 4.

3 Field Measurements

To illustrate the influence of local deviations in the nominal wheel–rail contact geometry on impact loading, a few results from various tests carried out in the field are summarised in this section. Field tests of dynamic wheel–rail interaction involving a train with different types of wheel irregularities (out-of-roundness) have been reported in several studies, see for example refs. [22–26].

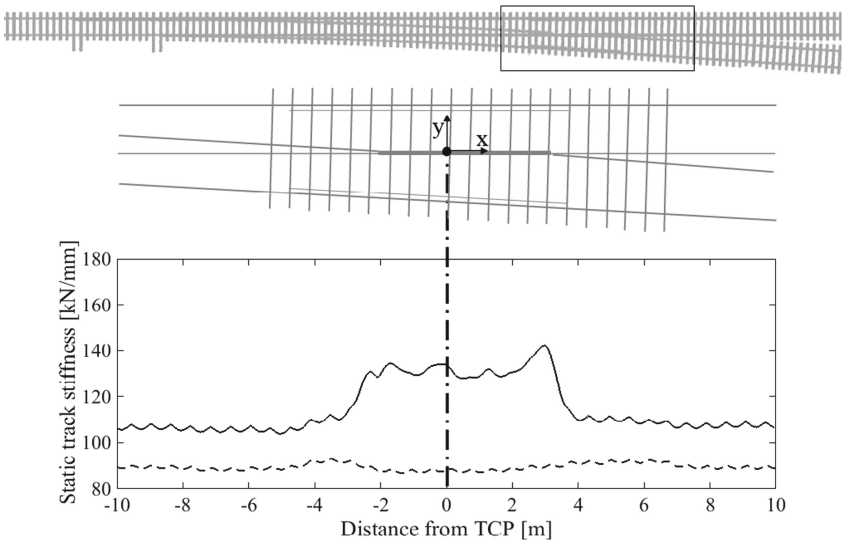

Fig. 4. Calculated static track stiffness at rail level along the through route in a crossing panel: — crossing rail, – – – outer rail. TCP indicates theoretical crossing point, i.e. the end of the crossing nose. From [21].

Results from one test are illustrated in Figs. 5 and 6 [23, 24]. Artificial wheel flats of length 40 mm and depth 0.35 mm were ground on the two wheels of one wheelset. The standard tangent track consisted of 60 kg/m rails, 10 mm studded rubber rail pads (here referred to as rail pad type A) and concrete monobloc sleepers on ballast. The standard rail pad with a dynamic stiffness of 120 kN/mm was replaced by a synthetic polymer-based pad (type B) along a track length of about 25 m. Laboratory measurements indicated that pad B was some ten times stiffer than pad A. The two test sites A and B were 70 m apart. An instrumented wheelset was used to measure the vertical wheel–rail contact force via strain gauges on the wheel discs [27]. The measured signals were low-pass filtered with cut-off frequency 1 kHz. An example of measured time history of the contact force is illustrated in Fig. 5 [23]. It is observed that the wheel flat results in a transient and periodic loading due to an impact for each revolution of the wheel. Initially, there is a partial unloading as the wheel flat enters the wheel–rail contact. During this phase, the wheel moves downwards (and the rail upwards) to compensate for the missing wheel material. Since the wheel and rail cannot completely compensate for the irregularity due to their inertia, there is a reduction in the contact force. After passing the centre of the flat, the wheel continues downwards because of its higher inertia. This results in a peak in the contact force, which is followed by a damped transient response.

The maximum contact force deviation from the static wheel load versus train speed is plotted in Fig. 6 for two different axle loads. Depending on the combination of rail pad stiffness and axle load, there is a local maximum at a speed between 20 and 70 km/h. Similar local maxima in wheel–rail contact force were reported in refs. [22, 26]. The local maximum is referred to as the P2 resonance [26], which can be described as the resonance frequency at which the unsprung mass of the vehicle and the equivalent track

mass are vibrating in phase on the equivalent stiffness of the track. This corresponds to the fundamental frequency at which the combined receptance of the coupled vehicle–track system has a local minimum. The unsprung mass of the vehicle includes the mass of the wheelset with axle boxes and parts of the primary suspension, and if present the brake discs and parts of the mechanical drive system. In Fig. 6, the local maximum (at both test sites) is shifted to a higher vehicle speed when the axle load is increased. This appears to be explained by the higher stiffness of the rail support with increasing axle load.

The influence on the wheel–rail impact load in a crossing of train speed, route and traffic direction has been investigated in a field test, see ref. [28]. Also here, the contact force was measured using an instrumented wheelset. For all train routes, an increase in impact load with increasing train speed was observed. For a given speed, the magnitude of the impact load was considerably higher for the diverging route compared with the through route. Based on the results from another field test with vehicle speeds in the range 40–70 km/h (and different types of rail pads than in Fig. 6) [29], it was concluded that the magnitude of the impact load in the crossing was reduced when implementing softer rail pads.

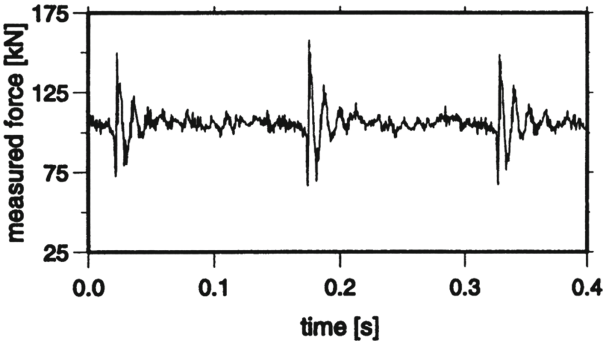

Fig. 5. Time history of wheel–rail contact force measured by an instrumented wheelset with a 40 mm rounded wheel flat. Vehicle speed 70 km/h and axle load 22 tonnes. From [23].

Pass-by noise and rail vibration generated by passenger trains in a fixed crossing (in the trailing move) have been measured [30, 31]. Noise was recorded using a microphone positioned at 7.5 m from the track centre and 1.2 m above the top of the rail. Vertical rail vibration was measured using an accelerometer attached to the underside of the wing rail at the position at which the wheel–rail contact transfers to the wing rail. Fig. 7 shows an example of measured rail vibration during a train passage, where the influence of the passing wheels can be observed as periodic maxima. However, these impacts were found to be less evident in the sound pressure signal. The spectrograms of the measured rail velocity and sound pressure are shown in Fig. 8. In the vibration data, the spectrogram is mainly characterised by horizontal bands. These correspond to each wheel impact and cause the rail to vibrate in a wide frequency range, with most of the energy concentrated between 20 and 1000 Hz. In contrast, the sound pressure spectrogram is mainly characterised by vertical bands. These are caused by the wheel/rail acoustic

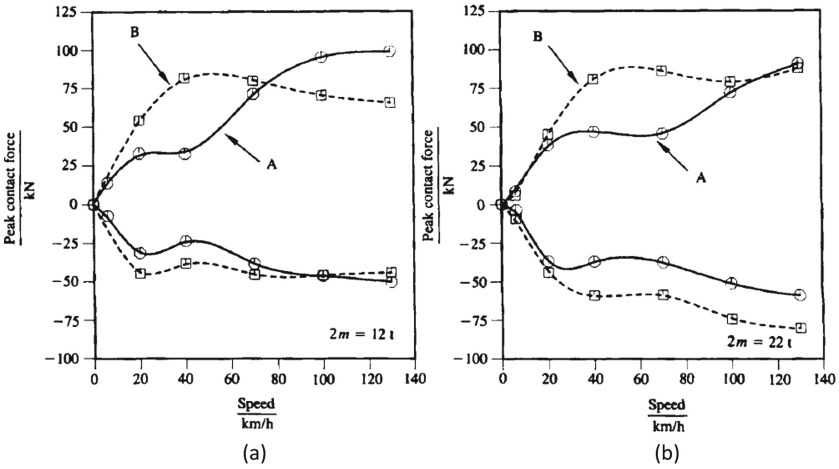

Fig. 6. Measured peak (maximum and minimum) contact force deviations from static wheel load versus train speed due to a 40 mm long wheel flat at test sites A and B for axle load (a) 12 tonnes and (b) 22 tonnes. From [24].

roughness and correspond to the rolling noise generated on the approach to and departure from the crossing. The acoustic roughness was measured as part of these tests and found to be much higher on the wing rail than outside the crossing, probably because grinding trains do not access the crossing. It was not possible to separate the rolling noise and impact noise and, although clearly audible, it was concluded that the contribution of the impact noise to the sound pressure spectra was small [31].

Results from a field test aiming to quantify the contribution of impact noise generated by different types of wheel tread defects on the pass-by noise of freight trains are presented in ref. [32]. The noisiest wheel with a 2 mm deep local crushing defect on the running surface led to an increased pass-by noise level (L_{Aeq} over the vehicle length) of 9 dB(A), measured at 7.5 m from a track with low acoustic roughness for train speeds 80–120 km/h. Wheel flats of depth 0.8 mm and 1.35 mm led to increases in noise level of 3 and 7 dB(A) respectively.

In ref. [33], a laboratory experiment was carried out in an anechoic chamber to examine the subjective reaction of 25 subjects to train noise containing components due to wheel–rail impact. Compared with railway noise without impact loading and at the same equivalent sound energy level, it was concluded that their recorded case of wheel flat noise increased the perceived loudness by 3 dB while the rail joint increased the loudness by 5 dB.

4 Quasi-Static Wheel Centre Vertical Trajectory – Point Contact Model

As discussed above, when the wheel runs over a discrete wheel/rail surface irregularity, this may lead to unloading of the wheel–rail contact and even a momentary loss of contact followed by the generation of an impact load. In a ‘point contact’ model, the

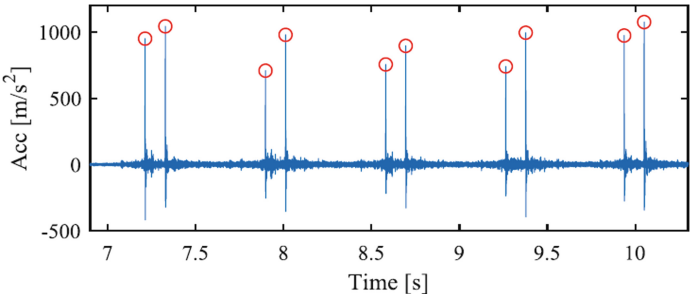

Fig. 7. Measured vertical acceleration of the wing rail. From [31].

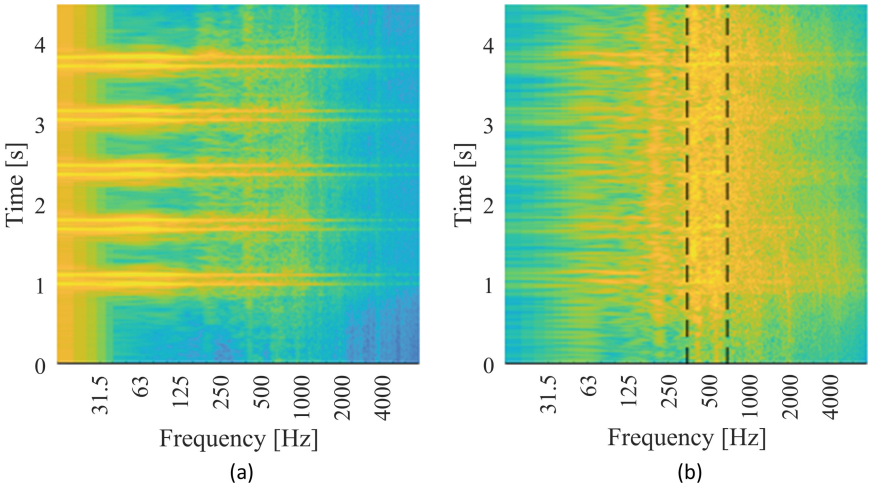

Fig. 8. Measured (a) rail vibration and (b) sound pressure spectrograms due to impact on the wing rail. From [31].

excitation of the wheel–rail system can be described by a relative displacement input between the wheel and rail that is equal to the quasi-static wheel centre trajectory, i.e., the path followed by the wheel centre if it ran very slowly over the surface irregularity [34]. In this section, expressions are presented for the quasi-static wheel centre trajectory, based on a simplified description of the geometry of each irregularity and assuming point contact between a rigid wheel and a rigid track. These formulae represent the prescribed relative wheel–rail vertical displacement excitation that occurs between a flexible wheel and a flexible track in the same way as the acoustic roughness, processed to account for the curvature of the wheel as described in EN 15610 [35], forms the input for rolling noise calculations [34, 36]. The actual motion of the wheel is the dynamic response to this excitation.

Although the simplified formulae given here are instructive in establishing trends of impact force, noise and vibration and their dependence on defect geometry, the actual geometry of the surface irregularity can vary considerably and will have a significant

influence on the magnitude of the impact load [37], see also Sect. 6.2. When using a three-dimensional contact model, the actual geometry of the surface irregularity serves as input to the calculation of the dynamic vehicle–track interaction [37]. In this case, the quasi-static wheel centre trajectory is not needed.

In this section, the contact filter effect on the input to the prescribed relative wheel–rail vertical displacement excitation is neglected, whereas it is automatically included if a three-dimensional elastic contact model is used. The influence of the contact model on the calculated impact load for new and rounded wheel flats will be discussed in Sect. 6.2.

4.1 Wheel Flat

In most models of wheel–rail interaction due to wheel flats, the two-dimensional shape of the flat is described by a simple analytical function. A new wheel flat with sharp edges can be described as a chord of the wheel circumference, where the length l_0 and depth d are approximately related by

$$l_0 \approx \sqrt{8R_w d} \tag{1}$$

Here R_w is the wheel radius and it is assumed that $d \ll R_w$. The vertical wheel profile deviation x_{nf}, which is the difference between the rolling surface of the undamaged wheel and the surface of the wheel featuring the new flat, is approximately given as, [37],

$$x_{nf} \approx d - \frac{z^2}{2R_w}, \quad -\frac{l_0}{2} \le z \le \frac{l_0}{2} \tag{2}$$

where z is the circumferential distance from the centre of the flat. As discussed in Sect. 2.1, the initial flat is soon transformed into a longer flat due to wear and plastic deformation of the flat edges. Based on ref. [22], the vertical wheel profile deviation x_{rf} for a rounded flat can be approximated as

$$x_{rf} = \frac{d}{2}\left(1 + \cos\left(\frac{2\pi z}{l}\right)\right), \quad -\frac{l}{2} \le z \le \frac{l}{2} \tag{3}$$

Here it is assumed that the depth of the new and rounded flats is the same but $l > l_0$, cf. Ref. [14]. The true two- and three-dimensional shapes of a wheel flat can be expected to be more complicated than indicated by Eqs. (2) and (3). In ref. [38], it is assumed that the three-dimensional shape of a new flat corresponds to the shape of the rail head on which it was formed. In this case, the parameter lines of the vertical wheel profile deviation in the rolling direction are of the type given in Eq. (2), while parameter lines in the transverse direction are circular arcs with rail head radius R_r.

Wheel flats introduce a relative displacement input to the wheel–rail system in a similar way as acoustic roughness. For a new flat, the wheel pivots around the two corners, and the wheel trajectory differs from the shape of the flat due to the curvature of the wheel. Assuming the rounded edges of the flat can be described by a quadratic function with smooth transitions and the lateral contact positions on the wheel and rail remain constant, the wheel centre vertical trajectory x_w can be written as, cf. Ref. [34],

$$x_w \approx \begin{cases} 4d\left((2z + l/2l)\right)^2, & -l/2 \le z \le 0 \\ 4d\left((l - 2z/2l)\right)^2, & 0 \le z \le l/2 \end{cases} \tag{4}$$

Note that Eq. (4) can be used also for new flats by using the relation $d = l^2/8R_w$, cf. Equation (1). Based on the wheel flat geometries described by Eqs. (2) and (3), examples of wheel centre trajectory for new and rounded wheel flats are given in Fig. 9. It is observed that the relative displacement excitation based on the vertical wheel centre trajectory differs from the geometric shape of the wheel flat. For the new flat in Fig. 9(a), it is observed that the slope of the wheel centre trajectory is discontinuous at the centre of the flat. This sharp discontinuity may have an influence on the magnitude of the impact load and a smoothing to account for the finite size of the contact (application of a contact filter) may be necessary, see Sect. 6.2.

For measured three-dimensional flats, a numerical procedure can be employed to determine the wheel centre trajectory, similar with that used in ref. [39] for roughness. The three-dimensional geometry of the flat and the lateral position of the running band relative to the centre of the flat influence the magnitude of the generated impact load. For example, in ref. [40] it was shown that the minimum circumferential curvature of the wheel tread along the wheel flat has a larger influence on the magnitude of the impact force than the flat depth.

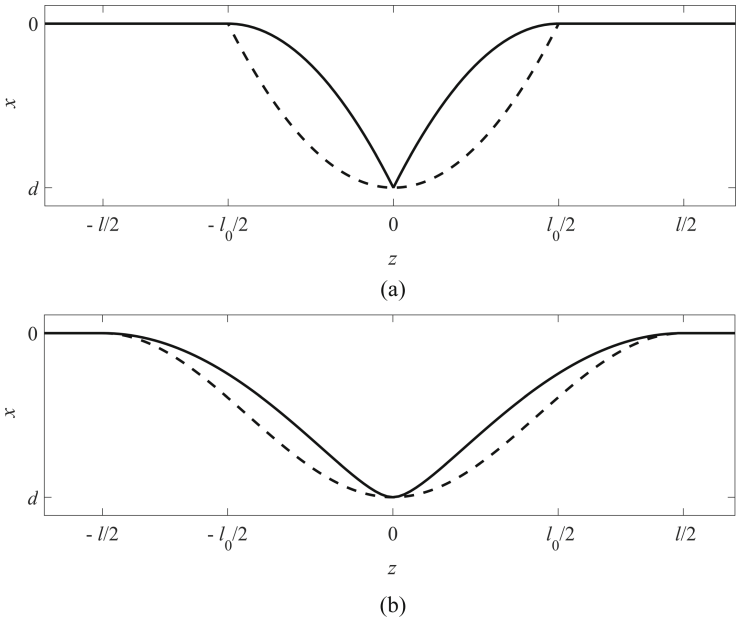

Fig. 9. Examples of relative displacement input: --- wheel profile deviation; – wheel centre trajectory: (a) new wheel flat with depth d and length l_0, (b) rounded wheel flat with depth d and length $l = 1.76l_0$. From [37].

4.2 Rail Joint

The corresponding equations for the relative vertical displacement excitation due to a rail joint were derived in ref. [41]. Again, this input is determined by the trajectory of

a rigid wheel over the rail joint on a rigid track. Three different situations may occur depending on whether the wheel is in tangential contact with the rail on either side of the joint when making the transition to the other rail. Depending on the type of contact at the transition, the three situations can be described as: (I) tangential contact on both sides of the gap, (II) tangential contact on one side and non-tangential contact on the other, and (III) non-tangential contact on both sides of the gap. The first two situations are illustrated in Fig. 10. Thus for situation II, for example, if the wheel is not in tangential contact with the rail when making first contact with the rail on the other side of the gap, it will pivot about the contact point on that rail edge until it regains tangential contact.

As discussed in Sect. 2.2, on each side of the joint, there is often a vertical dip in the rail. The geometry of the rail joint is then determined by the gap width w and height difference h between the two rail ends and by the geometry of the dip. Considering these input data, the geometry of each of the two rails ($i = 1, 2$) can be described by a set of coordinates (z_{ri}, x_{ri}). To determine the relative displacement excitation input, the position of the wheel when making simultaneous contact with both rails and the type of contact situation (I to III) need to be identified. This can be accomplished by applying a search algorithm around the unloaded joint, where the longitudinal position of the wheel on the left rail is shifted forwards in small steps until there is a first overlap between the wheel and the right rail. Based on the set of coordinates (z_{ri}, x_{ri}) and assuming continuous tangential contact on both rails (situation I in Fig. 10), the wheel centre trajectory (z_w, x_w) on either side of the joint is calculated as, [41],

$$\theta_i \approx \tan\theta_i = \frac{\mathrm{d}x_{ri}}{\mathrm{d}z_{ri}} \tag{5}$$

$$z_w = z_{ri} + R_w \sin\theta_i \tag{6}$$

$$x_w = x_{ri} + R_w(1 - \cos\theta_i) \tag{7}$$

However, if $\theta \geq \theta_2$ at the transition to the other rail (situation II in Fig. 10), the wheel will pivot around the rail end until it regains tangential contact. During this transition stage, the wheel centre trajectory is calculated as, [41],

$$z_w = z_r - R_w \sin\theta \tag{8}$$

$$x_w = x_r + R_w(1 - \cos\theta) \tag{9}$$

As in Sect. 4.1, it is assumed that the lateral contact positions on the wheel and rail profiles remain constant. Examples of wheel centre trajectory due to two different rail joints are shown in Fig. 11. Equations for the wheel centre trajectory in situation III are given in ref. [41], but it is stated that this is a situation that rarely occurs in practice. Furthermore, for gap widths $w \leq 20$ mm, it was concluded that the wheel centre trajectory is more influenced by the height difference than by the gap width.

4.3 Crossing

In front of the crossing nose (when observed in the facing move), the stock rail is curved laterally into the wing rail, see Fig. 3. In a facing move, this means that the contact

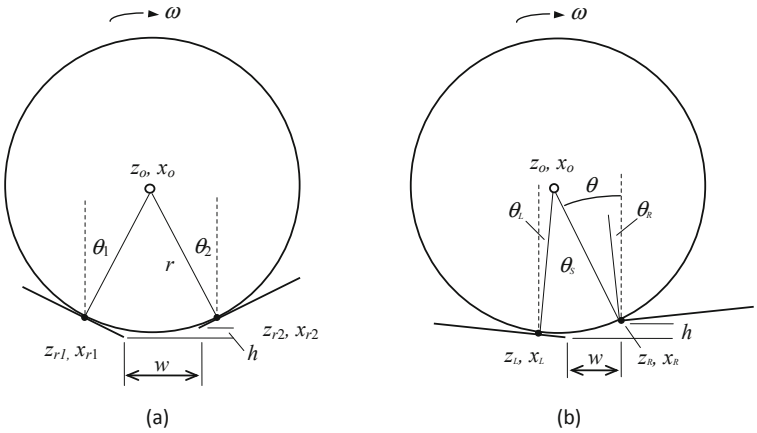

Fig. 10. Rolling contact geometry of a wheel over dipped rails at a joint: (a) situation I – tangential contact on both rails, (b) situation II – non-tangential contact on the right rail. From [41].

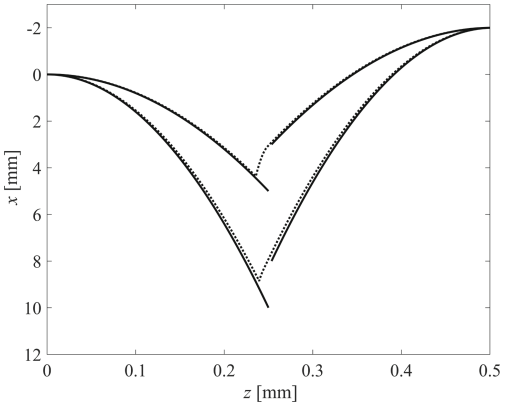

Fig. 11. Examples of relative displacement input for a wheel rolling over a dipped step-up rail joint with gap width $w = 7$ mm and vertical misalignment $h = 2$ mm: – dipped rail shape, --- wheel centre trajectory. Upper curves are for a 5 mm dip at the joint, bottom curves are for a 10 mm dip at the joint. From [41].

patch on the wheel tread moves outwards (away from the crossing nose) as long as the contact remains on the wing rail. Due to the decreasing wheel rolling radius, the wheel centre moves downwards until the wheel tread makes contact with the vertically inclined surface of the crossing nose. Due to this inclined surface, the wheel centre moves upwards again until the level of the stock rail is reached again (on the through rail). In contrast with Sects. 4.1 and 4.2, where it was assumed that the lateral contact position on the wheel profile remained constant, there is a significant variation in lateral contact positions on wheel and rail as the wheel passes over the crossing. The wheel centre trajectory is therefore influenced by the given crossing geometry as well as the specific wheel profile.